Genetics in Medicine

ARTICLE

Inherited variants in *CHD3* show variable expressivity in Snijders Blok-Campeau syndrome

ARTICLE INFO

ABSTRACT

Purpose: Common diagnostic next-generation sequencing strategies are not optimized to identify inherited variants in genes associated with dominant neurodevelopmental disorders as causal when the transmitting parent is clinically unaffected, leaving a significant number of cases with neurodevelopmental disorders undiagnosed.

Methods: We characterized 21 families with inherited heterozygous missense or protein-truncating variants in *CHD3*, a gene in which de novo variants cause Snijders Blok-Campeau syndrome.

Results: Computational facial and Human Phenotype Ontology–based comparisons showed that the phenotype of probands with inherited *CHD3* variants overlaps with the phenotype previously associated with de novo *CHD3* variants, whereas heterozygote parents are mildly or not affected, suggesting variable expressivity. In addition, similarly reduced expression levels of CHD3 protein in cells of an affected proband and of healthy family members with a *CHD3* protein-truncating variant suggested that compensation of expression from the wild-type allele is unlikely to be an underlying mechanism. Notably, most inherited *CHD3* variants were maternally transmitted.

Conclusion: Our results point to a significant role of inherited variation in Snijders Blok-Campeau syndrome, a finding that is critical for correct variant interpretation and genetic counseling and warrants further investigation toward understanding the broader contributions of such variation to the landscape of human disease.

© 2022 by American College of Medical Genetics and Genomics. Published by Elsevier Inc.

Introduction

The availability of exome sequencing in clinical practice has greatly improved the yield of genetic diagnostics for individuals with neurodevelopmental disorders (NDDs). In particular, sequencing of proband-parent trios, followed by filtering for de novo[1] or biallelic variants,[2] has proven to be a powerful tool to identify causal variants in individuals with sporadic dominant and recessive NDDs. However, although de novo and biallelic variants explain a substantial proportion of cases with NDDs,[1,2] the majority remains undiagnosed.[3] Various factors may explain the difficulties in diagnosing these individuals, including variation in genes not yet associated with disease, polygenic inheritance, or variation in noncoding regions.[4] In addition, coding variants associated with reduced penetrance and variable expressivity may underlie unexplained NDD cases. Common diagnostic strategies to analyze next-generation sequencing data are not optimized to identify the contributions of these factors to disease. Whereas penetrance indicates the proportion of individuals with a particular variant with a phenotype, expressivity describes the variability in severity of the phenotype between individuals with this variant.[4] Variable expressivity can cause highly variable symptoms, even in severe disorders that are caused by variants with a large effect.[4,5]

Jet van der Spek and Joery den Hoed contributed equally.
*Correspondence and requests for materials should be addressed to Tjitske Kleefstra. *E-mail address:* Tjitske.Kleefstra@radboudumc.nl
A full list of authors and affiliations appears at the end of the paper.

In this study, we show variable expressivity for variation in *CHD3*. CHD3 is an adenosine triphosphate–dependent chromatin remodeling protein that serves as a core member of the Nucleosome Remodeling Deacetylase complex.[6] Heterozygous variants in *CHD3* have recently been shown to cause a neurodevelopmental syndrome with a variable phenotype, ranging from mildly to more severely affected cases (Snijders Blok-Campeau syndrome [SNIBCPS], OMIM #618205).[6,7] *CHD3* is extremely intolerant for both loss-of-function (LoF) and missense variation (probability of LoF intolerance = 1, observed/expected = 0.09 [0.05-0.15]; Z = 6.15, observed/expected = 0.5 [0.46–0.53]), suggesting haploinsufficiency as a possible disease mechanism. However, the large majority of cases diagnosed with SNIBCPS carry confirmed de novo missense variants or single amino acid in-frame deletion variants (51/55, 93% of cases),[6,7] clustering in the adenosine triphosphatase (ATPase)-helicase domain of the encoded protein and affecting its ATPase activity and/or chromatin remodeling functions, which could be consistent with a dominant-negative mechanism.[6]

We assembled a cohort of 21 families with inherited *CHD3* variants and used a combination of objectified in-depth clinical analyses, cell-based expression studies, and large population cohort analyses to confirm the association of inherited *CHD3* variants with SNIBCPS and to show that heterozygote parents, who were predominantly females, often have (very) mild phenotypes, showing variable expressivity.

Materials and Methods

Individuals and consent

The cohort presented in this study was assembled from hospitals and laboratories across the Netherlands, Germany, the United States, Slovenia, Australia, and Canada. Informed consent for the use and publication of medical data and biological material was obtained from all patients or their legal representative by the involved clinician. Consent for publication of photographs was obtained separately.

Next-generation sequencing

CHD3 variants in all probands were identified using exome sequencing or genome sequencing (families 4 and 12). According to the American College of Medical Genetics/Association for Molecular Pathology guidelines, all *CHD3* variants were classified as variants of uncertain significance (class III),[8] with inheritance from seemingly healthy/mildly affected parents combined with previously unreported reduced penetrance as an important criterion. Inheritance of variants was confirmed either as part of trio exome sequencing or using targeted Sanger sequencing after identification in singleton exon analysis. Similarly, if

applicable, other family members were tested using targeted sequencing.

Pathogenicity of missense variants was further evaluated using Combined Annotation Dependent Depletion-Phred v1.6,[9] PolyPhen-2,[10] and Sorting Intolerant From Tolerant annotation[11] scores. Allele frequencies of all variants in Genome Aggregation Database (GnomAD) were based on ENST00000330494.7.[12]

Facial analysis

We established a 2-dimensional hybrid facial model that combines the analysis of the Clinical Face Phenotype Space pipeline with the facial recognition system of the OpenFace pipeline.[13,14] First, we generated a 468-dimensional feature vector of the facial features of 30 individuals with de novo *CHD3* variants. After extraction of the hybrid features for each of the individuals, we calculated whether the individuals with de novo *CHD3* variants cluster together when compared with a group of matched controls on the basis of the nearest neighbor principle (Euclidean distance); these matched controls were individuals with intellectual disability (ID) and are age-, ethnicity-, and sex-matched. A Mann-Whitney U test was used to determine whether the clustering of individuals with de novo *CHD3* variants was significantly higher than expected on the basis of random chance. A *P*-value smaller than .05 was considered significant.

Furthermore, a classifier was built using a logistic regression model trained on the 468-dimensional feature vector of the 30 individuals. The performance was evaluated using leave-one-out cross validation, and the classifier was shown to have a sensitivity of 0.91, a specificity of 0.83, and an overall area under the receiver operating characteristic curve of 0.91. Finally, using the trained classifier, we determined for each inherited case whether that individual clusters within the de novo *CHD3* group or the control group.

Construction of composite face

For 13 individuals with an inherited *CHD3* variant and 30 with a de novo *CHD3* variant, facial 2-dimensional photographs were available for generating a composite face. As previously described, average faces were generated while allowing for asymmetry preservation and equal representation by individuals.[15]

Human Phenotype Ontology–based phenotype clustering analysis

We performed Human Phenotype Ontology (HPO)–based clustering analysis using 35 individuals with de novo *CHD3* variants,[6] 20 of 21 probands with an inherited *CHD3* variant, and 20 of 21 heterozygote parents in the analysis; the proband and heterozygote mother of

family 6 were excluded because no clinical data were available and the mother was mosaic for the *CHD3* variant (approximately 37%). The Wang score (a measure of semantic similarity) between all terms was calculated using the HPO Sim package.[16,17] The terms were divided into groups on the basis of the similarity score; a new feature—the sum of the terms in the group—was created as a replacement for the terms in that specific group (Supplemental Table 1). HPO terms that could not be added to a group feature were added as a separate term. To quantify and visualize possible differences in our cohort, we used Partitioning Around Medoids clustering on these grouped features. We compared probands with a de novo and inherited variant and probands with inherited variants and their heterozygote parents in a second analysis. To assess statistical significance, a permutations test ($n = 100,000$) was used with relabeling based on variant types while taking into account the original distribution of variant types.

Three-dimensional protein modeling

We modeled the protein structure of the ATPase-helicase domain of CHD3 in interaction with the DNA using the homology modeling script in the WHAT IF[18] and YASARA[19] Twinset with standard parameters. As a template, we used Protein Data Bank file 6RYR, which contains the human nucleosome–CHD4 complex structure of a single copy of CHD4.[20] The PHD2 variant (p.(S477F)) was modeled in the PHD2 domain of CHD4 (Protein Data Bank 2L75, 89% sequence identity with CHD3).[21]

DNA expression constructs and site-directed mutagenesis

The cloning of *CHD3* (NM_001005273.2/ENST0000033 0494.7) has been described previously.[6] The coding DNA sequence of *GATAD2B* (NM_020699.3/ENST00000368 655.4) and a C-terminal region of CHD3-encoding residues 1246 to 1944 (NM_001005273.2) were amplified using primers listed in Supplemental Table 2. Variants in full-length CHD3 or the C-terminal CHD3 construct were generated using the QuikChange Lightning Site-Directed Mutagenesis Kit (Agilent). The primers used for site-directed mutagenesis are listed in Supplemental Table 3. Complementary DNAs (cDNAs) were subcloned using BamHI/HpaI (full-length CHD3), BamHI/XbaI (GATAD2B), or HindIII/BamHI (C-terminal CHD3 construct) into pYFP, pHisV5, and pRluc, created by modification of the pEGFP-C2 vector (Clontech). All constructs were verified by Sanger sequencing.

Cell culture

Lymphoblastoid cell lines were established by Epstein-Barr virus transformation of peripheral lymphocytes from blood samples collected in heparin tubes and maintained in RPMI medium (Sigma-Aldrich) supplemented with 15% fetal bovine serum and 5% HEPES (both Invitrogen). HEK293T/17 cells (CRL-11268, American Type Culture Collection) were grown in DMEM supplemented with 10% fetal bovine serum and 1× penicillin-streptomycin (all Invitrogen) at 37 °C with 5% carbon dioxide. Transfections were performed using GeneJuice (Millipore) following the manufacturer's protocol.

Testing for nonsense-mediated decay of truncating variants

Lymphoblastoid cell lines of members of family 1 and controls were grown overnight with 100 μg/mL cycloheximide (Sigma-Aldrich) to block nonsense-mediated decay (NMD). After treatment, cell pellets were collected, and RNA and protein were extracted using the RNeasy Mini Kit (Qiagen) or with 1× RIPA buffer (Thermo Fisher Scientific) supplemented with 1% PMSF (Sigma-Aldrich) and 1× PIC (Roche), respectively. Reverse transcriptase–polymerase chain reaction was performed using SuperScript III Reverse Transcriptase (Thermo Fisher Scientific) with random primers, and regions of interest were amplified from cDNA using primers listed in Supplemental Table 4. Sanger trace peak sizes of the wild-type and variant alleles were measured using the "Area" option in ImageJ (National Institutes of Health), and proportion of the variant allele was calculated: peak area variant allele / (peak area variant + wild-type allele). Quantitative polymerase chain reactions were performed from cDNA with iQ SYBR Green supermix (Bio-Rad), using primers *CHD3-F* (5′-AGGAAGACCAAGACAACCAGTCAG-3′), *CHD3-R* (5′-TGACTGTCTACGCCCTTCAGGA-3′), *TBP-F* (5′-GG GCACCACTCCACTGTATC-3′), *TBP-R* (5′-CGAAGTG-CAATGGTCTTTAGG-3′), *PPIA-F* (5′-TATCTGCACTG CCAAGACTGAGTG-3′), and *PPIA-R* (5′-CTTCTTGCT GGTCTTGCCATTCC-3′).

Direct fluorescent imaging

HEK293T/17 cells were grown on coverslips coated with poly-D-lysine (Sigma-Aldrich). Forty-eight hours after transfection with the YFP-tagged C-terminal CHD3 construct and HisV5-tagged GATAD2B, cells were fixed with 4% paraformaldehyde (Electron Microscopy Sciences). Nuclei were stained with Hoechst 33342 (Invitrogen). Fluorescence images were acquired with a Zeiss LSM880 confocal microscope and Airyscan unit using ZEN Image Software (Zeiss).

Fluorescence recovery after photobleaching assays

HEK293T/17 cells were transfected in clear-bottomed black 96-well plates with YFP-tagged full-length CHD3 or

p.(S477F). After 48 hours, medium was replaced with phenol red-free DMEM supplemented with 10% fetal bovine serum (both Invitrogen), and cells were moved to a temperature-controlled incubation chamber at 37 °C. Fluorescent recordings were acquired using Zeiss LSM880 and Zen Black Image Software, with alpha Plan-Apochromat 100×/1.46 Oil DIC M27 objective (Zeiss). Fluorescence recovery after photobleaching experiments were performed by photobleaching an area of 0.98 μm × 0.98 μm within a single nucleus with 488-nm light at 100% laser power for 3 iterations with a pixel dwell time of 32.97 μs, followed by collection of times series of 150 images with a 2.5 zoom factor and an optical section thickness of 1.4 μm (2.0 Airy units). Individual recovery curves were background subtracted and normalized to the prebleach values, and mean recovery curves were calculated using EasyFRAP software.[22] Curve fitting was done with FrapBot application using direct normalization and a single component exponential model to calculate the half-time and maximum recovery.[23]

Immunoblotting

Whole-cell lysates were collected in 1× RIPA buffer supplemented with 1× PIC and 1% PMSF. Cells were lysed for 20 minutes at 4 °C followed by centrifugation for 20 minutes at 12,000 rpm. Samples were loaded on 4% to 15% Mini-PROTEAN TGX Precast Gels (Bio-Rad) and transferred onto polyvinylidene fluoride membranes. Membranes were blocked in 5% milk for 1 hour at room temperature and then probed with rabbit anti-CHD3 antibody (1:1000; Abcam, ab109195) or mouse anti-GFP (1:8000; Clontech, 632380) overnight at 4 °C. Next, membranes were incubated with horseradish peroxidase–conjugated goat anti-rabbit or goat anti-mouse antibody (1:10,000; Jackson ImmunoResearch) for 1.5 hours at room temperature. Bands were visualized with the SuperSignal West Femto Maximum Sensitivity Substrate Reagent Kit (CHD3; Thermo Fisher Scientific) or the Novex ECL Chemiluminescent Substrate Reagent Kit (YFP-fusion proteins; Invitrogen) using ChemiDoc XRS + System (Bio-Rad).

Coimmunoprecipitation

HEK293T/17 cells were transfected with the YFP-tagged C-terminal region of CHD3 and Rluc-tagged GATAD2B. After 48 hours, whole-cell lysates were collected in Pierce IP Lysis Buffer (25 mM Tris-HCl pH 7.4, 150 mM NaCl, 1 mM EDTA, 1% NP-40, and 5% glycerol; Thermo Fisher Scientific) supplemented with 1× PIC and 1% PMSF. Cells were lysed for 20 minutes at 4 °C followed by centrifugation for 20 minutes at 12,000 rpm. YFP-fusion proteins were immobilized on GFP-trap magnetic agarose beads (ChromoTek) overnight at 4 °C. Deactivated beads (ChromoTek) were used as a negative control. The elutions and 5% of the

input were resolved on 4% to 15% Mini-PROTEAN TGX Precast Gels (Bio-Rad) and transferred onto polyvinylidene fluoride membranes. Membranes were blocked in 5% milk for 1 hour at room temperature and then probed with rabbit anti-Rluc antibody (1:2000; GeneTex) overnight at 4 °C. Next, membranes were incubated with horseradish peroxidase–conjugated goat anti-rabbit antibody (1:10,000; Jackson ImmunoResearch) for 1.5 hours at room temperature. Bands were visualized with the SuperSignal West Femto Maximum Sensitivity Substrate Reagent Kit (Thermo Fisher Scientific) using ChemiDoc XRS + System (Bio-Rad).

Population-based analysis of the association of CHD3 variation with intelligence, educational qualification, and intracranial volume/head circumference

Using exome sequencing data of 200,000 individuals from the UKB Exome Sequencing Consortium[24] (J.D. Szustakowski et al, unpublished, and https://www.ukbiobank.ac.uk/media/cfulxh52/uk-biobank-exome-release-faq_v9-december-2020.pdf), we studied the association of CHD3 missense and putative LoF variants with "Fluid intelligence score" (data field ID 3533), "Qualifications" (data field ID 6138), and "Volume of Estimated Total Intra Cranial" (data field ID 7054). In addition, we used genome-wide association meta-analysis summary statistics of head circumference (HC) ($n \leq 18{,}881$) and HC combined with intracranial volume ($n \leq 45{,}458$) in childhood and adulthood[25] and infant HC ($n \leq 10{,}768$)[26] to calculate gene-level P-values reflecting the common variant associations of CHD3 with these traits using Multi-marker Analysis of Genomic Annotation.[27] For detailed description of the methods, see Supplemental Notes 1.

Results

Phenotypic features in probands with inherited *CHD3* variants overlap with the SNIBCPS phenotype

We identified 21 families with SNIBCPS, each initially identified through a proband diagnosed with a syndromic NDD carrying a rare inherited *CHD3* missense variant ($n = 13$) or protein-truncating variant (PTV) ($n = 8$) (NM_001005273.2/ENST00000330494.7) (Figure 1, Supplemental Figure 1). Per clinical observations, all probands had phenotypes overlapping with the SNIBCPS phenotype associated with de novo variants in *CHD3* (Figure 2, Supplemental Figure 2, Table 1, Supplemental Notes 2, Supplemental Tables 5 and 6). Computational facial analysis also confirmed the presence of a SNIBCPS facial gestalt in probands (Supplemental Figure 3,
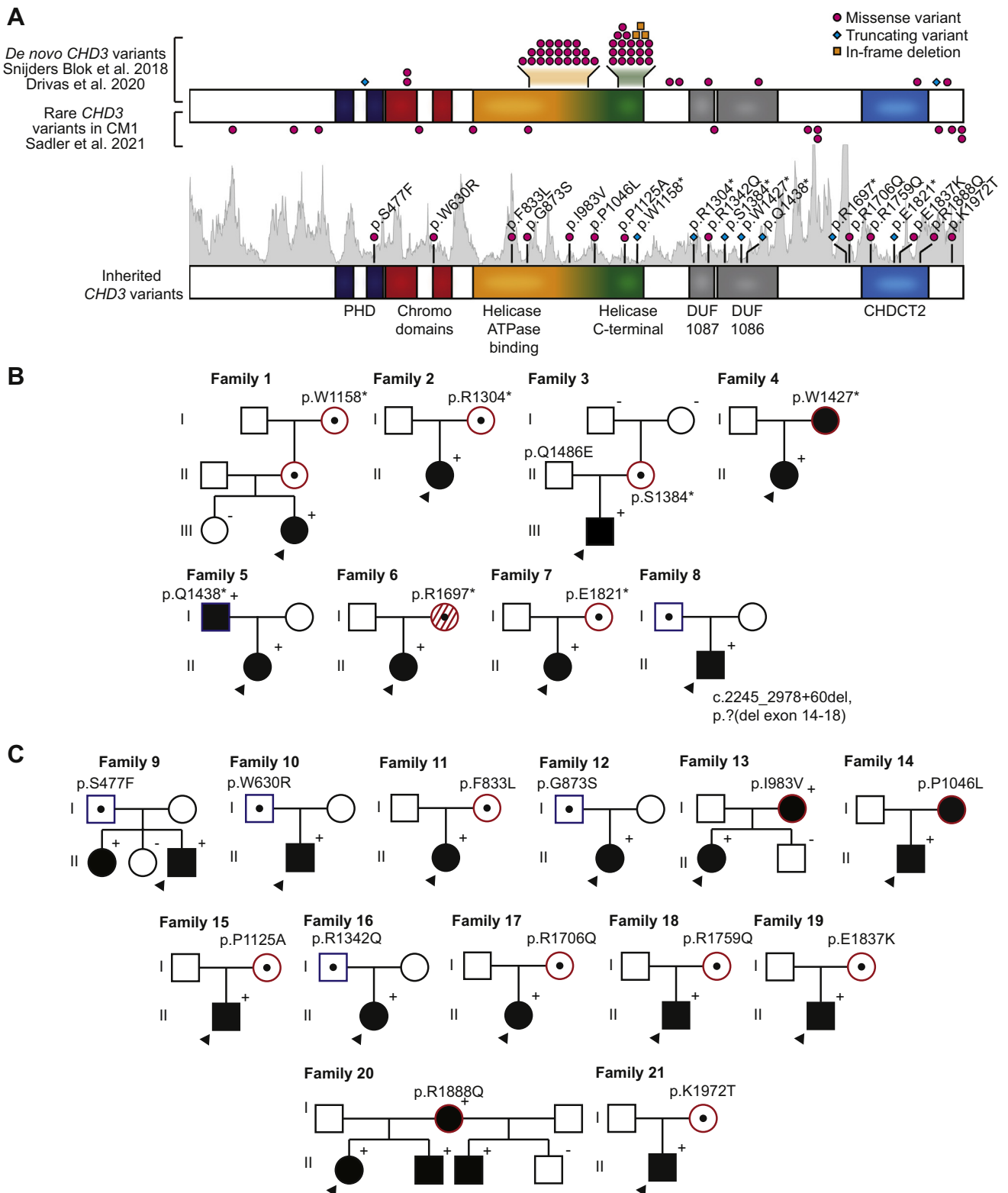
Figure 1 **Twenty-one families with inherited *CHD3* variants.** A. Schematic representation of the CHD3 protein (NM_001005273.2/ NP_001005273.2), including functional domains, with protein-truncating variants labeled as cyan diamonds, in-frame deletions as orange squares, and missense variants as magenta circles. The intolerance landscape, which was visualized using MetaDome[28] and computed on the basis of single-nucleotide variants in the Genome Aggregation Database, showing per amino acid position the missense over synonymous ratio, is shaded in gray. The top schematic shows de novo *CHD3* variants identified in individuals with neurodevelopmental disorders reported in Snijders Blok et al [6] and Drivas et al,[7] and rare variants associated with CM1 reported in Sadler et al.[29] The bottom schematic presents cases with inherited *CHD3* variants described in this study. B, C. Pedigrees of families identified with inherited *CHD3* variants, in

Supplemental Table 6), and composite images showed similarities in facial features between probands with de novo and inherited *CHD3* variants (squared face, deep-set eyes, pointed chin) (Figure 2B).

In-depth phenotypic analysis of probands with inherited *CHD3* variants and their heterozygote parents

For 17 heterozygote parents (17/21, 81%), phenotypic information minimally regarding development and dysmorphisms was available. All parents had at least 1 feature of SNIBCPS (Supplemental Table 6). In 5 parents (5/17, 29%), this was limited to only 1 (families 1 and 10) or 2 phenotypic features (families 9, 16, and 21) (Supplemental Table 6). Whereas most heterozygote parents (16/17, 94%) presented with a single (eg, prominent forehead or deep-set eyes) or several facial features known in SNIBCPS and 50% (8/16) had macrocephaly (Table 1, Supplemental Table 6), the parents had either mild/borderline ID (4/19, 21%) or no history of ID (15/19, 79%) (Table 1, Supplemental Tables 4 and 6, Supplemental Notes 2). Taken together, these observations suggest a combination of both variable expressivity and reduced penetrance for these rare genetic variations in *CHD3*.

We more objectively compared the phenotypes of probands with de novo and inherited *CHD3* variants on the basis of HPO terminology,[30] using a Partitioning Around Medoids clustering algorithm. Although this computational analysis did not identify a phenotypic difference between probands with de novo and inherited variants (31/55 individuals clustered correctly, $P = .44771$) (Figure 2C, Supplemental Figure 4), it confirmed a phenotypic difference between probands with inherited *CHD3* variants and their heterozygote parents (33/40 individuals clustered correctly, $P < .00001$) (Figure 2C, Supplemental Figure 4).

Maternal transmission of inherited *CHD3* variants is predominant

We noticed that most variants in our cohort were maternally inherited (15/21, 71%, $P = .0392$, 1-sided binomial test with expected ratios of 0.5 for paternal and 0.5 for maternal inheritance) (Figure 1B and C, Supplemental Figure 5A). For single-nucleotide variants with a LoF effect, 6 of 7 (86%, $P = .0625$) variants were maternally inherited (Figure 1B, Supplemental Figure 5A). Notably, the only father transmitting a LoF single-nucleotide variant was affected (mild ID). This observation could hint at a female-protective effect

for genetic variation in *CHD3*. However, we did not observe a sex bias in the affected probands (12/21 female, $P > .9999$) or more severe ID in male than in female de novo or inherited cases.[6,7] To further explore the hypothesis of a female-protective effect at population level, we analyzed all *CHD3* LoF variants in GnomAD (15/198,800 individuals) and found that a significantly higher number of these variants were present in females than in males (12/15, $P = .0173$, 2-sided Fisher's exact test) (Supplemental Figure 5B).

Effects of an inherited *CHD3* PTV on transcript and protein expression levels

Few cases with SNIBCPS have been described with confirmed de novo *CHD3* PTVs (4/55, 7.3% of cases),[6,7] including one that is predicted to escape NMD (NP_001005273.1:p.[Phe1935GlufsTer108]). However, in our study, we identified 7 families with inherited single-nucleotide PTVs and 1 with an intragenic deletion with a predicted LoF effect (8/20, 40%) (Figure 1A). None of the inherited PTVs were predicted to escape NMD. We functionally confirmed this in family 1 (Figure 3A), for which we treated lymphoblastoid cell lines from the proband (individual III-2), heterozygote mother (II-2) and grandmother (I-2), and the healthy sibling of the proband who did not carry the variant (III-1) with cycloheximide to inhibit NMD, followed by direct amplification and Sanger sequencing of the *CHD3* transcript. We found that treatment with cycloheximide increased expression of the mutant allele, showing that the NM_001005273.2:c.3473G>A variant was targeted by NMD in all samples, as expected (Figure 3B).

An explanation for variable expressivity of PTVs could be compensation of expression by the wild-type allele to maintain normal expression levels. To test whether such compensation plays a role in variable expressivity of *CHD3* PTVs, we evaluated the expression of the *CHD3* variant in family 1 (c.3473G>A, p.[W1158*]) on a transcript and protein level. We found that this variant resulted in lower levels of *CHD3* transcript and CHD3 protein in lymphoblastoid cells from individuals I-2, II-2, and III-2 compared to the levels observed in cells from the healthy sibling who did not carry the variant (individual III-1; Figure 3C and D). These findings confirm the LoF effect of the stop-gain variant in this family and make it unlikely that compensation by the wild-type allele is an underlying mechanism for the milder phenotype in the heterozygote mother and grandmother.

(B) families with predicted loss-of-function (LoF) variants and (C) families with missense variants. The arrowhead indicates the proband, filled symbols represent affected individuals (defined as individuals with developmental delay and/or intellectual disability), open symbols with a central dot represent confirmed heterozygotes without developmental delay/intellectual disability, and "+" is used for a confirmed familial *CHD3* variant and "−" for individuals confirmed not to carry the variant. Symbols with red contours represent female heterozygotes, and symbols with blue contours represent male heterozygotes. The dashed symbol for family 6 represents mosaic state of the variant in the mother. In pedigrees, only genetically tested siblings of the proband are shown. ATPase, adenosine triphosphatase; CM1, Chiari I malformations; DUF, domain of unknown function.
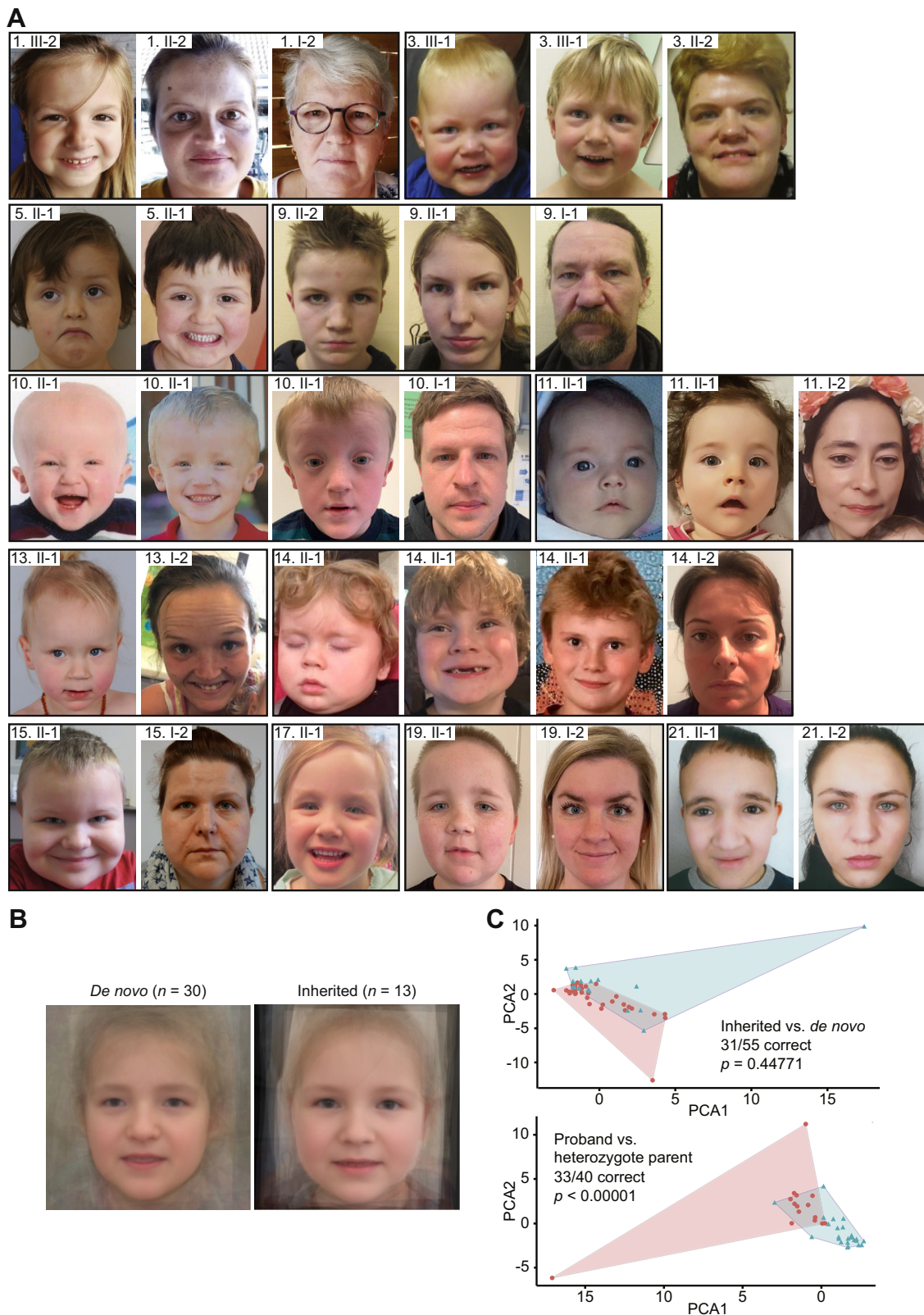
Figure 2   Facial features and clinical evaluation of individuals with inherited *CHD3* variants. A. Facial photographs of individuals with inherited *CHD3* variants. Individuals show features also observed in individuals with de novo *CHD3* variants, including a squared appearance of the face, prominent forehead, widely spaced eyes, thin upper lip, pointed chin, and deep-set eyes. These characteristics are also present in heterozygote parents. As observed previously, facial gestalt changes with age.[7] For example, a prominent nose is especially seen in adult individuals. For childhood pictures of heterozygote parents, see Supplemental Figure 2. B. Computational average of facial photographs of 30 individuals with de novo *CHD3* variants (left) and 13 probands with inherited *CHD3* variants (right). C. Partitioning Around Medoids

In silico and functional analyses of inherited *CHD3* missense variants

In addition to the 7 inherited *CHD3* single-nucleotide PTVs and the intragenic deletion, we identified 13 families with inherited missense variants. One of the identified inherited missense variants, also present in an unaffected heterozygote parent, was identical to a variant previously reported as a de novo variant in an individual with SNIBCPS (p.[R1342Q]; individual 32 in Snijders Blok et al[6]). On the basis of the phenotypes observed in the probands with inherited *CHD3* missense variants, the conservation of affected positions (Supplemental Figure 1), and in silico predictions of pathogenicity (Supplemental Figure 6, Supplemental Table 5), we considered these inherited *CHD3* missense variants as likely pathogenic with variable expressivity in the parents. Clinically, probands carrying a *CHD3* missense variant did not seem to be more severely affected than individuals with PTVs (Supplemental Table 7). We followed up on the inherited missense variants using cell-based functional assays to test for chromatin binding (for p.[S477F]) and GATAD2B binding (for p.[R1342Q], p.[E1837K], and p.[Q1888R]) but did not find evidence that these protein functions were affected (Supplemental Figure 5).

Rare *CHD3* variants in a large population cohort

The presence of rare, likely pathogenic *CHD3* variants in healthy individuals prompted us to study possible effects of variation in this gene at a population level, using data from the UK Biobank resource[24,31-34] and J.D. Szustakowski et al (unpublished). For a detailed description of these analyses, see Supplemental Notes 1. These analyses were limited to White British ancestry. First, we found no associations between rare missense variation at variation-intolerant locations in *CHD3* (minor allele frequency $\leq 1\%$, located in functional domains, damaging in PolyPhen or Sorting Intolerant From Tolerant annotation, and with Combined Annotation Dependent Depletion-Phred score > 25) and fluid intelligence ($n = 77,998$), educational qualification ($n = 120,596$), or intracranial volume ($n = 18,254$). We then tested for group differences for these 3 phenotypes between individuals with and those without rare putative *CHD3* LoF variants. At nominal significance, we observed a larger intracranial volume in individuals with rare *CHD3* putative LoF variants ($n = 4$, $t = 2.37$, $P = .018$). We note that this result does not remain significant after a conservative Bonferroni correction for testing of 3 different phenotypes (adjusted $P = .054$). However, in light

of the observed macrocephaly in 47% to 53% of probands with a (likely) pathogenic *CHD3* variant and in 50% of heterozygote parents (Table 1) and the link of rare *CHD* variants with abnormal brain growth,[29] the potential convergence of findings in the 4 individuals with *CHD3* LoF variants in this independent population cohort is intriguing. To test possible relationships between *CHD3* common genetic variation and HC and/or intracranial volume, we performed gene-level analyses using previously published single-nucleotide polymorphism-wise association summary statistics for these traits,[25,26] but none of the results survived multiple testing correction (Supplemental Notes 1).

Discussion

In the present study, we used inherited variation to show variable expressivity for SNIBCPS. The phenotypic spectrum of individuals with an inherited *CHD3* variant ranged from moderate ID combined with multiple other features to only a single facial feature or macrocephaly. Additional evidence for variable expressivity for *CHD3* variation is provided by the recently identified association of 19 rare *CHD3* missense variants with Chiari I malformations in individuals without features of SNIBCPS (Figure 1A).[29] It is important to note that, although younger generations seem more severely affected than previous generations, this may be caused by ascertainment bias.[35]

The female predominance we observed among the heterozygote parents in our cohort and for individuals with *CHD3* LoF variants in GnomAD could indicate a female protective effect for *CHD3* variation. Previous studies have repeatedly shown a male bias in NDDs, a higher pathogenic variant burden in females, and a maternal transmission bias in rare inherited variants,[3,36,37] suggesting that female sex protects against genetic variation in disease. This phenomenon might contribute to the variable expressivity observed for the inherited *CHD3* variants.

Using transcript and protein expression studies, we found significantly lower CHD3 expression levels in 3 family members carrying a *CHD3* PTV, independent of whether or not these individuals were affected with ID. Hence, we found no evidence for compensatory expression by the wild-type allele in blood-derived cells. However, it remains to be determined whether such LoF variance can have a tissue-specific, temporal expression–specific, and/or transcript-specific effect. It is unclear whether results from blood-derived cells can be extrapolated to neuronal cell types, which would be more relevant considering the NDD

---

analyses of clustered Human Phenotype Ontology–standardized clinical data from 35 individuals with de novo *CHD3* variants, 20 affected probands with an inherited variant, and 20 heterozygote parents. The analyses do not show a significant distinction between the clusters of probands with de novo and probands with inherited variants (upper graph; $P = .44771$). There is, however, a significant difference between the clusters of affected probands with inherited variants and heterozygote parents (bottom graph; $P < .00001$). PCA, principal component analysis.

Table 1 Summary of phenotypes seen in individuals with *CHD3* variants

Phenotypic Feature	Probands With De Novo Variant[a]	Probands With Inherited Variant	Heterozygote Parents
Development			
Developmental delay	100% (55/55)	100% (21/21)	17% (3/18)
Intellectual disability	98% (46/47)	79% (11/14)	21% (4/19)
Borderline/borderline-mild	6% (3/47)	14% (2/14)	11% (2/18)
Mild/mild-moderate	30% (14/47)	29% (4/14)	6% (1/18)
Moderate/moderate-severe	36% (17/47)	14% (2/14)	0% (0/18)
Severe	23% (11/47)	0% (0/14)	0% (0/18)
Level unknown	2% (1/47)	21% (3/14)	6% (1/18)
Speech delay/disorder	100% (53/53)	100% (20/20)	24% (4/17)
Autism or autism-like features	35% (18/51)	53% (10/19)	18% (3/17)
Neurology			
Hypotonia	81% (39/48)	89% (17/19)	17% (2/12)
Macrocephaly	53% (28/53)	47% (9/19)	50% (8/16)
CNS abnormalities	50% (24/48)	62% (8/13)	25% (1/4)
Neonatal feeding problems	31% (10/32)	21% (4/19)	6% (1/16)
Facial dysmorphisms			
High/broad/prominent forehead	85% (28/33)	85% (17/20)	53% (9/17)
Thin upper lip	79% (15/19)	55% (11/20)	47% (8/17)
Widely spaced eyes	69% (35/51)	70% (14/20)	24% (4/17)
Broad nasal bridge	75% (15/20)	80% (16/20)	24% (4/17)
Full cheeks	58% (11/19)	70% (14/20)	13% (2/16)
Pointed chin	60% (12/20)	53% (10/19)	41% (7/17)
Deep-set eyes	55% (11/20)	47% (9/19)	50% (8/16)
Other			
Joint laxity (generalized and/or local)	36% (18/50)	40% (8/20)	29% (4/14)
Vision problems	72% (38/53)	25% (5/20)	53% (8/15)
Male genital abnormalities	32% (8/25)	22% (2/9)	0% (0/4)
Hernia (umbilical, inguinal, hiatal)	13% (6/48)	10% (2/20)	0% (0/14)

CNS, central nervous system.

[a]Combined cases from Snijders Blok et al[6] and Drivas et al[7] (confirmed de novo only).

phenotypes in our cohort, especially given that neuron-specific alternative splicing has previously been described for *CHD3*.[38]

Other explanations for the clinical variable expressivity of inherited *CHD3* variants include the presence of a second hit on the other allele by either rare or common variation, a genome-wide higher mutational burden of high-penetrant variants, or common variants in promoter/enhancer regions or in other genes, inherited from the parent who did not transmit the inherited *CHD3* variant.[4,39] Such a compound inheritance mechanism has, eg, been described for thrombocytopenia-absent radius syndrome, in which the inheritance of a rare null allele together with 1 of 2 low-frequency single-nucleotide polymorphisms in regulatory regions causes disease.[40] In 4 probands with an inherited *CHD3* variant, a copy number variant was also reported, including 1 22q11.2 duplication, which has been described with highly variable features (OMIM #608363), and 3 copy number variants of uncertain significance (Supplemental Table 5). Proband 7 had other (likely) pathogenic variants contributing to the phenotype (Supplemental Table 5, Supplemental Notes 2). A comparison with the prevalence of additional genetics finding in individuals with de novo *CHD3* variants could

not be made owing to lack of reporting on additional genetic findings.[6,7]

The individuals with de novo missense variants published to date were mostly (although not entirely) localized to the ATPase-helicase domain.[6,7] No clustering in the ATPase-helicase domain or elsewhere was observed among the inherited missense variants of our cohort (Figure 1A). It has been speculated that the de novo missense variants clustering in the ATPase-helicase domain are unlikely to lead to a sole LoF effect[6] and may potentially act in a dominant-negative way. The identification of 8 families with an inherited LoF variant and the lack of clustering of the inherited missense variants may suggest a LoF effect as the main mechanism for inherited cases, which may underlie the variable expressivity. However, our cell-based analyses did not find evidence of LoF for the protein functions that we tested (Supplemental Figure 7). This does not exclude that these variants have an effect on other biological functions of CHD3. According to 3-dimensional protein modeling, the previously published de novo missense variants within the ATPase-helicase domain localize more closely to the ATP binding site than the inherited missense variants of our cohort (Supplemental Notes 3). Interestingly, the p.(I983V) (family 13) variant was found to be closer to
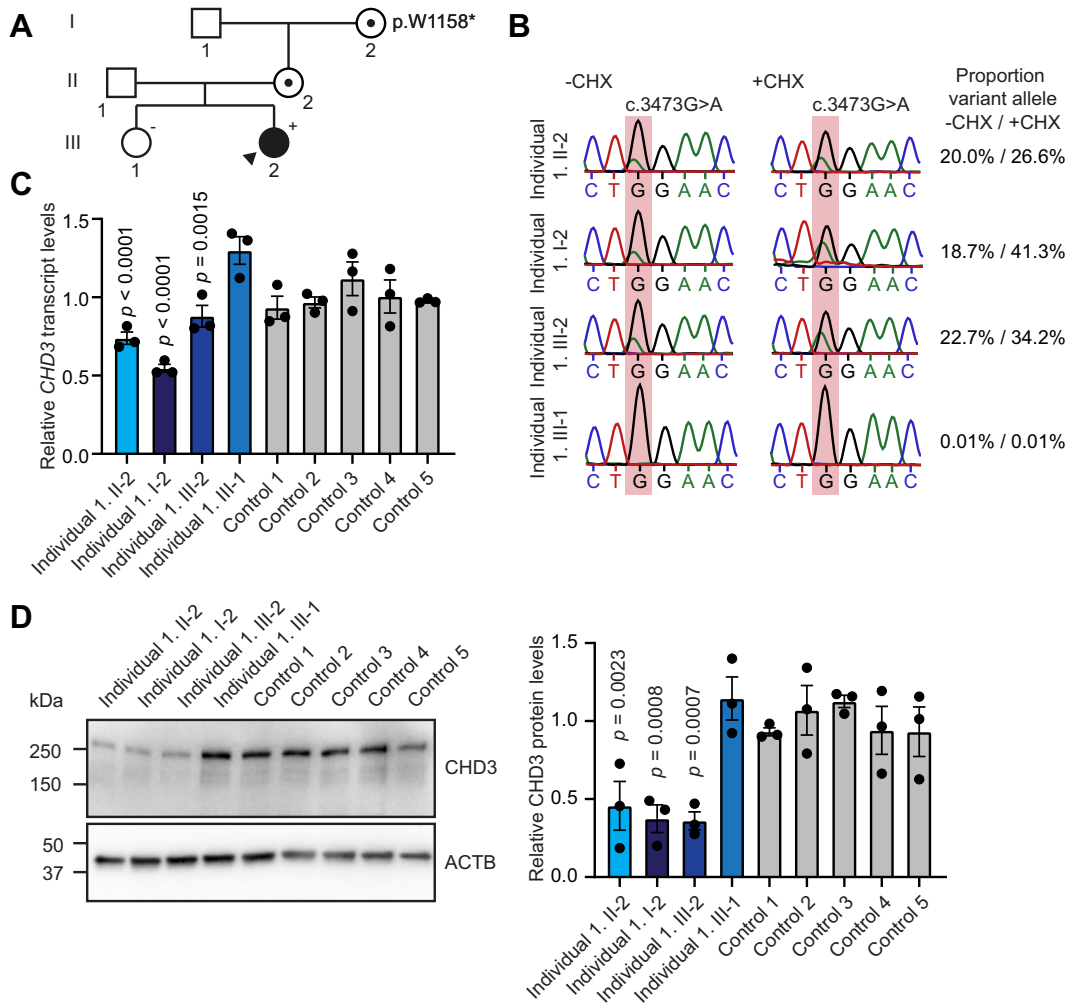
Figure 3 **Functional consequences of the *CHD3* p.(W1158*) protein-truncating variant in subject-derived lymphoblastoid cell lines.** A. Pedigree of family identified with an inherited *CHD3* c.3473G>A, p.(W1158*) variant. B. Sanger sequencing chromatographs of Epstein-Barr virus (EBV)-immortalized lymphoblastoid cell lines derived from members of family 1. Individuals I-2, II-2, and III-2 carried the c.3473G>A, p.(W1158*) variant, and individual III-1 was a healthy sibling who did not carry the variant. Cells were treated with (+CHX) or without cycloheximide (–CHX) to test for nonsense-mediated decay (NMD). The mutated position is shaded in red. The transcript carrying the variant allele is present at lower levels than the wild-type allele and increases after CHX treatment (proportion variant allele calculated as: peak area variant allele / [peak area variant + wild-type allele]), showing that this variant is targeted by NMD. C. Quantitative polymerase chain reaction of EBV-immortalized lymphoblastoid cell lines of family 1 (shades of blue) and 5 unrelated controls (gray) for *CHD3* transcript levels (NM_001005273.2). Values are normalized to expression of *PPIA* and *TBP* and shown relative to unrelated controls. Bars represent mean ± SEM with individual data points plotted ($n = 3$; P-values compared with individual III-1 [healthy sibling who did not carry the variant], one-way analysis of variance [ANOVA] [sum-of-squares (within) = 0.2660, sum-of-squares (between) = 1.098], and posthoc Bonferroni test). D. Left: A representative immunoblot of protein lysates prepared from lymphoblastoid cell lines for CHD3 (expected molecular weight: approximately 227 kDa). The blot was probed for ACTB to ensure equal protein loading. Right: A graph showing the quantification of immunoblots with bars presenting mean ± SEM and individual data points plotted ($n = 3$; P-values compared with individual III-1 [healthy sibling who did not carry the variant], one-way ANOVA [sum-of-squares (within) = 0.7852, sum-of-squares (between) = 2.528] and posthoc Bonferroni test). Controls are shaded in gray, and samples from family 1 are shaded in blue. C, D. The cell lines carrying c.3473G>A, p.(W1158*) show lower *CHD3* transcript/protein levels than the control samples.

published de novo variants (Supplemental Notes 3), and the heterozygote parent with this missense variant did have a neurodevelopmental phenotype that was more pronounced than in other heterozygote parents (Figures 1C and 2, Supplemental Table 6, Supplemental Notes 2).

With the identification and characterization of inherited *CHD3* variants with variable expressivity in 21 families, we

showed that, in addition to highly penetrant de novo variants, rare predicted likely pathogenic inherited variants in *CHD3* should be considered as possibly pathogenic depending on variant characteristics in cases with phenotypic concordance to SNIBCPS. Interestingly, variable penetrance and expressivity has been noted in numerous families with another dominant NDD, KBG syndrome,

caused by LoF variants in *ANKRD11* (OMIM #148050).[41] So, this phenomenon is likely more common for dominant NDDs, with important implications for clinical genetic counseling, in the context of recurrence risk, prenatal diagnostics, prognosis, and variant interpretation.

Clinically, we recommend that it can be helpful to evaluate the parents of children with *CHD3* variants for subtle SNIBCPS features. In particular, macrocephaly and facial dysmorphisms, including a prominent forehead and pointed chin, could be recognized in a substantial number of heterozygote parents (50% and 94%, respectively) (Figure 2A, Supplemental Table 6). Taken together, our results illustrate the continuum of causality for NDDs with genetic origins[36,42] and significantly underline the hypothesis that variable expressivity and reduced penetrance likely explain a large portion of as yet unexplained NDD cases. Overall, we show that even for genes already known to be implicated in an NDD, inherited variation and variable expressivity can play a major role, and are thus important to consider in genetic counseling.

Data Availability

All data sets generated and analyzed during the current study are available from the corresponding author on request.

Acknowledgments

Author Information

Conceptualization: J.v.d.S., J.d.H., L.S.B., C.G., H.G.B., T.K.; Formal Analysis: J.v.d.S., J.d.H., A.J.M.D., D.S.; Investigation: J.v.d.S., J.d.H.; Methodology: J.v.d.S., J.d.H. L.S.B.; Resources: T.S.B., E.M.B., S.B.-W., G.B., N.J.B., T.B., P.M.C. G.C., T.B.H., I.H., R.A.H., B.K., S.C.L., L.L., J.M., A.M., V.M., D.C.M., C.W.O., L.S.P., V.P., L.R., C.R., A.R., E.M.C.S., M.E.H.S., S.S., T.Y.T, M.L.T, E.J.W., M.H.W.; Software: A.J.M.D., D.S., C.N., H.V., G.D.N.A.; Supervision: T.K., S.E.F. L.E.L.M.V., B.B.A.d.V.; Visualization: J.v.d.S., J.d.H.; Writing-Original Draft: J.v.d.S., J.d.H.; Writing-Review and Editing: T.K., S.E.F., L.E.L.M.V., C.F.

Ethics Declaration

All study proceedings involving humans were in compliance with the principles set out in the Declaration of Helsinki. This study was approved by the Institutional Review Board "Commissie Mensgebonden Onderzoek Regio Arnhem-Nijmegen" under number 2011/188. Written informed consent for the use and publication of medical data and biological material was obtained from all individuals or their legal representative by the involved clinician. Written informed consent for publication of photographs was obtained specifically and separately. This study includes data from the UK Biobank Study (http://www.ukbiobank.ac.uk).[30] UK Biobank received ethical approval from the NHS National Research Ethics Service North West (11/NW/0382) and had obtained informed consent from all participants. The current analyses were conducted under UK Biobank data application number 16066.

Conflict of Interest

M.L.T. is an employee of HudsonAlpha Institute for Biotechnology. For D.M., the following statements are applicable: "Research disclaimer: The views expressed in

Additional Information

The online version of this article (https://doi.org/10.1016/j.gim.2022.02.014) contains supplementary material, which is available to authorized users.

Authors

Jet van der Spek[1,2], Joery den Hoed[3,4],
Lot Snijders Blok[1,2,3], Alexander J.M. Dingemans[1,2],
Dick Schijven[3], Christoffer Nellaker[5,6,7], Hanka Venselaar[8],
Galuh D.N. Astuti[1,9], Tahsin Stefan Barakat[10],
E. Martina Bebin[11], Stefanie Beck-Wödl[12], Gea Beunders[13],
Natasha J. Brown[14,15], Theresa Brunet[16],
Han G. Brunner[1,2,17], Philippe M. Campeau[18,19],
Goran Čuturilo[20,21], Christian Gilissen[1,22],
Tobias B. Haack[12], Irina Hüning[23], Ralf A. Husain[24],
Benjamin Kamien[25], Sze Chern Lim[14], Luca Lovrecic[26],
Janine Magg[27], Ales Maver[26], Valancy Miranda[18,19],
Danielle C. Monteil[28], Charlotte W. Ockeloen[1],
Lynn S. Pais[29], Vasilica Plaiasu[30], Laura Raiti[14],
Christopher Richmond[14,31,32], Angelika Rieß[12],
Eva M.C. Schwaibold[33], Marleen E.H. Simon[34],
Stephanie Spranger[35], Tiong Yang Tan[14,15],
Michelle L. Thompson[36], Bert B.A. de Vries[1,2],
Ella J. Wilkins[14], Marjolein H. Willemsen[1],
Clyde Francks[3,37], Lisenka E.L.M. Vissers[1,2],
Simon E. Fisher[3,37], Tjitske Kleefstra[1,2,38,*] (iD)

Affiliations

[1]Department of Human Genetics, Radboud University Medical Center, Nijmegen, The Netherlands; [2]Donders Institute for Brain, Cognition and Behaviour, Radboud University Medical Center, Nijmegen, The Netherlands; [3]Department of Language and Genetics, Max Planck Institute for Psycholinguistics, Nijmegen, The Netherlands; [4]International Max Planck Research School for Language Sciences, Max Planck Institute for Psycholinguistics, Nijmegen, The Netherlands; [5]Nuffield Department of Women's and Reproductive Health, University of Oxford, Women's Centre, John Radcliffe Hospital, Oxford, United Kingdom; [6]Department of Engineering Science, Institute of Biomedical Engineering, University of Oxford, Oxford, United Kingdom; [7]Big Data Institute, Li Ka Shing Centre for Health Information and Discovery, University of Oxford, Oxford, United Kingdom; [8]Center for Molecular and Biomolecular Informatics, Radboud University Medical Center, Nijmegen, The Netherlands; [9]Division of Human Genetics, Center for Biomedical Research (CEBIOR), Faculty of Medicine, Diponegoro University, Semarang, Indonesia; [10]Department of Clinical Genetics, Erasmus MC University Medical Center, Rotterdam, The Netherlands; [11]Department of Neurology, University of Alabama at Birmingham, Birmingham, AL; [12]Department of Medical Genetics and Applied Genomics, University of Tübingen, Tübingen, Germany; [13]Department of Genetics, University Medical Center Groningen, Groningen, The Netherlands; [14]Victorian Clinical Genetics Services, Murdoch Children's Research Institute, Parkville, Victoria, Australia; [15]Department of Pediatrics, University of Melbourne, Royal Children's Hospital, Parkville, Victoria, Australia; [16]Institute of Human Genetics, School of Medicine, Technical University Munich, Munich, Germany; [17]Department of Clinical Genetics, Maastricht University Medical Center, GROW School for Oncology and Developmental Biology, and MHeNS School for Mental health and Neuroscience, Maastricht University, Maastricht, The Netherlands; [18]CHU Sainte-Justine Research Center, Montreal, Quebec, Canada; [19]Sainte-Justine Hospital, University of Montreal, Montreal, Quebec, Canada; [20]University Children's Hospital Belgrade, Belgrade, Serbia; [21]Faculty of Medicine, University of Belgrade, Belgrade, Serbia; [22]Department of Human Genetics, Radboud Institute for Molecular Life Sciences, Radboud University Medical Center, Nijmegen, The Netherlands; [23]Institute of Human Genetics, University of Lübeck, Lübeck, Germany; [24]Department of Neuropediatrics, Jena University Hospital, Jena, Germany; [25]Genetic Services of Western Australia, King Edward Memorial Hospital, Perth, Western Australia, Australia; [26]Clinical Institute for Genomic Medicine, University Medical Center Ljubljana, Ljubljana, Slovenia; [27]Department of Neuropaediatrics, Developmental Neurology, Social Pediatrics, University Children's Hospital, University of Tübingen, Tübingen, Germany; [28]Department of Pediatrics, Naval Medical Center Portsmouth, Portsmouth, VA; [29]Broad Institute Center for Mendelian Genomics, Broad Institute of MIT and Harvard, Cambridge, MA; [30]INSMC Alessandrescu-Rusescu, Regional Center of Medical Genetics Bucharest, Bucharest, Romania; [31]Genetic Health Queensland, Royal Brisbane and Women's hospital, Herston, Queensland, Australia; [32]School of Medicine, Griffith University, Southport, Queensland, Australia; [33]Institute of Human Genetics, Heidelberg University, Heidelberg,

Germany; [34]Department of Medical Genetics, University Medical Center Utrecht, Utrecht, The Netherlands; [35]Praxis für Humangenetik-Bremen, Bremen, Germany; [36]HudsonAlpha Institute for Biotechnology, Huntsville, AL; [37]Donders Institute for Brain, Cognition and Behaviour, Radboud University, Nijmegen, Netherlands; [38]Center of Excellence for Neuropsychiatry, Vincent van Gogh Institute for Psychiatry, Venray, The Netherlands

References

1. Deciphering Developmental Disorders Study. Prevalence and architecture of de novo mutations in developmental disorders. *Nature*. 2017;542(7642):433–438. http://doi.org/10.1038/nature21062.
2. Martin HC, Jones WD, McIntyre R, et al. Quantifying the contribution of recessive coding variation to developmental disorders. *Science*. 2018;362(6419):1161–1164. http://doi.org/10.1126/science.aar6731.
3. Kaplanis J, Samocha KE, Wiel L, et al. Evidence for 28 genetic disorders discovered by combining healthcare and research data. *Nature*. 2020;586(7831):757–762. http://doi.org/10.1038/s41586-020-2832-5.
4. Castel SE, Cervera A, Mohammadi P, et al. Modified penetrance of coding variants by cis-regulatory variation contributes to disease risk. *Nat Genet*. 2018;50(9):1327–1334. http://doi.org/10.1038/s41588-018-0192-y.
5. Chen R, Shi L, Hakenberg J, et al. Analysis of 589,306 genomes identifies individuals resilient to severe Mendelian childhood diseases. *Nat Biotechnol*. 2016;34(5):531–538. http://doi.org/10.1038/nbt.3514.
6. Snijders Blok L, Rousseau J, Twist J, et al. CHD3 helicase domain mutations cause a neurodevelopmental syndrome with macrocephaly and impaired speech and language. *Nat Commun*. 2018;9(1):4619. Published correction appears in *Nat Commun*. 2019;10(1):883. Published correction appears in *Nat Commun*. 2019;10(1):2079. https://doi.org/10.1038/s41467-018-06014-6
7. Drivas TG, Li D, Nair D, et al. A second cohort of CHD3 patients expands the molecular mechanisms known to cause Snijders Blok-Campeau syndrome. *Eur J Hum Genet*. 2020;28(10):1422–1431. http://doi.org/10.1038/s41431-020-0654-4.
8. Richards S, Aziz N, Bale S, et al. Standards and guidelines for the interpretation of sequence variants: a joint consensus recommendation of the American College of Medical Genetics and Genomics and the Association for Molecular Pathology. *Genet Med*. 2015;17(5):405–424. http://doi.org/10.1038/gim.2015.30.
9. Rentzsch P, Witten D, Cooper GM, Shendure J, Kircher M. CADD: predicting the deleteriousness of variants throughout the human genome. *Nucleic Acids Res*. 2019;47(D1):D886–D894. http://doi.org/10.1093/nar/gky1016.
10. Adzhubei IA, Schmidt S, Peshkin L, et al. A method and server for predicting damaging missense mutations. *Nat Methods*. 2010;7(4):248–249. http://doi.org/10.1038/nmeth0410-248.
11. Vaser R, Adusumalli S, Leng SN, Sikic M, Ng PC. SIFT missense predictions for genomes. *Nat Protoc*. 2016;11(1):1–9. http://doi.org/10.1038/nprot.2015.123.
12. Karczewski KJ, Francioli LC, Tiao G, et al. The mutational constraint spectrum quantified from variation in 141,456 humans. *Nature*. 2020;581(7809):434–443. Published correction appears in *Nature*. 2021;590(7846):E53. Published correction appears in *Nature*. 2021;597(7874):E3-E4. https://doi.org/10.1038/s41586-020-2308-7
13. Dingemans AJM, Stremmelaar DE, van der Donk R, et al. Quantitative facial phenotyping for Koolen-de Vries and 22q11.2 deletion syndrome. *Eur J Hum Genet*. 2021;29(9):1418–1423. http://doi.org/10.1038/s41431-021-00824-x.
14. van der Donk R, Jansen S, Schuurs-Hoeijmakers JHM, et al. Next-generation phenotyping using computer vision algorithms in rare genomic neurodevelopmental disorders. *Genet Med*. 2019;21(8):1719–1725. http://doi.org/10.1038/s41436-018-0404-y.
15. Reijnders MRF, Miller KA, Alvi M, et al. De novo and inherited loss-of-function variants in TLK2: clinical and genotype-phenotype evaluation of a distinct neurodevelopmental disorder. *Am J Hum Genet*. 2018;102(6):1195–1203. http://doi.org/10.1016/j.ajhg.2018.04.014.
16. Deng Y, Gao L, Wang B, Guo X. HPOSim: an R package for phenotypic similarity measure and enrichment analysis based on the human phenotype ontology. *PLoS One*;10(2):e0115692. https://doi.org/10.1371/journal.pone.0115692
17. Wang JZ, Du Z, Payattakool R, Yu PS, Chen CF. A new method to measure the semantic similarity of GO terms. *Bioinformatics*. 2007;23(10):1274–1281. http://doi.org/10.1093/bioinformatics/btm087.
18. Vriend G. WHAT IF: a molecular modeling and drug design program. *J Mol Graph*. 1990;8(1):52-56, 29 https://doi.org/10.1016/0263-7855(90)80070-v.
19. Krieger E, Koraimann G, Vriend G. Increasing the precision of comparative models with YASARA NOVA–a self-parameterizing force field. *Proteins*. 2002;47(3):393–402. http://doi.org/10.1002/prot.10104.
20. Farnung L, Ochmann M, Cramer P. Nucleosome-CHD4 chromatin remodeler structure maps human disease mutations. *Elife*. 2020;9:e56178. http://doi.org/10.7554/eLife.56178.
21. Mansfield RE, Musselman CA, Kwan AH, et al. Plant homeodomain (PHD) fingers of CHD4 are histone H3-binding modules with preference for unmodified H3K4 and methylated H3K9. *J Biol Chem*. 2011;286(13):11779–11791. http://doi.org/10.1074/jbc.M110.208207.
22. Koulouras G, Panagopoulos A, Rapsomaniki MA, Giakoumakis NN, Taraviras S, Lygerou Z. EasyFRAP-web: a web-based tool for the analysis of fluorescence recovery after photobleaching data. *Nucleic Acids Res*. 2018;46(W1):W467–W472. http://doi.org/10.1093/nar/gky508.
23. Kohze R, Dieteren CEJ, Koopman WJH, Brock R, Schmidt S. Frapbot: an open-source application for FRAP data. *Cytometry A*. 2017;91(8):810–814. http://doi.org/10.1002/cyto.a.23172.
24. Van Hout CV, Tachmazidou I, Backman JD, et al. Exome sequencing and characterization of 49,960 individuals in the UK Biobank. *Nature*. 2020;586(7831):749–756. http://doi.org/10.1038/s41586-020-2853-0.
25. Haworth S, Shapland CY, Hayward C, et al. Low-frequency variation in TP53 has large effects on head circumference and intracranial volume. *Nat Commun*. 2019;10(1):357. http://doi.org/10.1038/s41467-018-07863-x.
26. Taal HR, Pourcain BS, Thiering E, et al. Common variants at 12q15 and 12q24 are associated with infant head circumference. *Nat Genet*. 2012;44(5):532–538. http://doi.org/10.1038/ng.2238.
27. de Leeuw CA, Mooij JM, Heskes T, Posthuma D. MAGMA: generalized gene-set analysis of GWAS data. *PLoS Comput Biol*. 2015;11(4):e1004219. http://doi.org/10.1371/journal.pcbi.1004219.
28. Wiel L, Baakman C, Gilissen D, Veltman JA, Vriend G, Gilissen C. MetaDome: pathogenicity analysis of genetic variants through aggregation of homologous human protein domains. *Hum Mutat*. 2019;40(8):1030–1038. http://doi.org/10.1002/humu.23798.
29. Sadler B, Wilborn J, Antunes L, et al. Rare and de novo coding variants in chromodomain genes in Chiari I malformation. *Am J Hum Genet*. 2021;108(1):100–114. Published correction appears in *Am J Hum Genet*. 2021;108(2):368. Published correction appears in *Am J Hum Genet*. 2021;108(3):530-531 https://doi.org/10.1016/j.ajhg.2020.12.001.
30. Köhler S, Carmody L, Vasilevsky N, et al. Expansion of the Human Phenotype Ontology (HPO) knowledge base and resources. *Nucleic Acids Res*. 2019;47(D1):D1018–D1027. http://doi.org/10.1093/nar/gky1105.
31. Sudlow C, Gallacher J, Allen N, et al. UK Biobank: an open access resource for identifying the causes of a wide range of complex diseases of middle and old age. *PLoS Med*. 2015;12(3):e1001779. http://doi.org/10.1371/journal.pmed.1001779.
32. Bycroft C, Freeman C, Petkova D, et al. The UK Biobank resource with deep phenotyping and genomic data. *Nature*. 2018;562(7726):203–209. http://doi.org/10.1038/s41586-018-0579-z.

33. Alfaro-Almagro F, Jenkinson M, Bangerter NK, et al. Image processing and quality control for the first 10,000 brain imaging datasets from UK Biobank. *Neuroimage*. 2018;166:400–424. http://doi.org/10.1016/j.neuroimage.2017.10.034.

34. Miller KL, Alfaro-Almagro F, Bangerter NK, et al. Multimodal population brain imaging in the UK Biobank prospective epidemiological study. *Nat Neurosci*. 2016;19(11):1523–1536. http://doi.org/10.1038/nn.4393.

35. Wright CF, West B, Tuke M, et al. Assessing the pathogenicity, penetrance, and expressivity of putative disease-causing variants in a population setting. *Am J Hum Genet*. 2019;104(2):275–286. http://doi.org/10.1016/j.ajhg.2018.12.015.

36. Jacquemont S, Coe BP, Hersch M, et al. A higher mutational burden in females supports a "female protective model" in neurodevelopmental disorders. *Am J Hum Genet*. 2014;94(3):415–425. http://doi.org/10.1016/j.ajhg.2014.02.001.

37. Duyzend MH, Nuttle X, Coe BP, et al. Maternal modifiers and parent-of-origin bias of the autism-associated 16p11.2 CNV. *Am J Hum Genet*. 2016;98(1):45–57. http://doi.org/10.1016/j.ajhg.2015.11.017.

38. Porter RS, Jaamour F, Iwase S. Neuron-specific alternative splicing of transcriptional machineries: implications for neurodevelopmental disorders. *Mol Cell Neurosci*. 2018;87:35–45. http://doi.org/10.1016/j.mcn.2017.10.006.

39. Girirajan S, Rosenfeld JA, Coe BP, et al. Phenotypic heterogeneity of genomic disorders and rare copy-number variants. *N Engl J Med*. 2012;367(14):1321–1331. Published correction appears in *N Engl J Med*. 2012;367(24):2362. https://doi.org/10.1056/NEJMoa1200395

40. Albers CA, Paul DS, Schulze H, et al. Compound inheritance of a low-frequency regulatory SNP and a rare null mutation in exon-junction complex subunit RBM8A causes TAR syndrome. *Nat Genet*. 2012;44(4):435–439, S1-S2. http://doi.org/10.1038/ng.1083.

41. Low K, Ashraf T, Canham N, et al. Clinical and genetic aspects of KBG syndrome. *Am J Med Genet A*. 2016;170(11):2835–2846. http://doi.org/10.1002/ajmg.a.37842.

42. Katsanis N. The continuum of causality in human genetic disorders. *Genome Biol*. 2016;17(1):233. http://doi.org/10.1186/s13059-016-1107-9.